An in-line dye tracer experiment to measure the residence time in continuous concrete processing

Materials and Structures (2024) 57:104
https://doi.org/10.1617/s11527-024-02378-y

ORIGINAL ARTICLE

An in-line dye tracer experiment to measure the residence time in continuous concrete processing

Arjen Deetman · Derk Bos · Jan Blaakmeer · Theo Salet · Sandra Lucas

Received: 9 February 2024 / Accepted: 25 April 2024

Abstract This paper introduces an in-line dye tracer experiment to measure the residence time functions in continuous concrete processing. These functions quantify the material-system interdependency and can be used to compare different material-system combinations and for quality and process control. A Rhodamine B solution was used as the tracer material and detected by measuring the color intensity using a digital image processing technique. The experiment was validated on a 3D concrete printing system by comparing the results of impulse, step-up and step-down inputs with different tracer quantities. The results show that a high signal-to-noise ratio can be obtained with low tracer concentrations. For the examined combination of material and system, an impact on the original process was only observed for the step-up inputs at high tracer quantities. It is concluded that the presented method is cost-effective and non-labor-intensive and, therefore, has the potential for wide adoption and integration in automated workflows.

Keywords Tracer experiment · 3d concrete printing · Residence time distribution · Digital image processing · Color dye · Rhodamine B

1 Introduction

Recently, new high-tech concrete manufacturing methods have been developed, such as Smart Dynamic Casting [1], 3D concrete printing [2], and shotcrete printing [3]. These methods completely or partially remove the need for formwork. To overcome the lack of support from the formwork, the material strength and stiffness need to increase with increasing building height [4–6]. This increase is commonly achieved with accelerating or rheology-modifying additives [7–9]. Depending on the strategy, additive, bulk material and system, these are added to the dry mixture or water, or the wet concrete just before placement [10]. Since the material is commonly required to be pumped before placement, which conflicts with the required shape-stable properties after placement, the production process is more time-sensitive than production methods that use formwork [11].

The material properties depend on material composition (cement, water, sand, aggregates, additives, and others) and the system parameters (mixing time, residence time, shear rate, pressure, temperature, and others). Therefore, the material and system must be jointly designed to obtain the desired behavior [12, 13]. However, a quantitative understanding of the

A. Deetman (✉) · D. Bos · T. Salet · S. Lucas
Department of the Built Environment, Eindhoven University of Technology, P.O. Box 513, 5600 MB Eindhoven, The Netherlands
e-mail: a.h.deetman@tue.nl

J. Blaakmeer
Saint-Gobain Weber Beamix, Hastelweg 161, 5652 CJ Eindhoven, The Netherlands

Published online: 17 May 2024

interdependency between material and system is still lacking, even though this understanding is needed to develop further and compare existing combinations of materials and systems. One parameter that can quantify the interdependency is the residence time distribution (RTD), whose importance has already been acknowledged [10, 14]. This frequency distribution of residence time represents the flow of a material through a system and is thus influenced by both the material and the system properties [15]. The RTD is a parameter to compare the behavior of different materials in a system and the behavior of the same material in different systems. It might (partially) explain why certain materials are well suited for specific systems and behave differently in others. It can be used as one of the parameters to conduct comparative studies between research labs and industrial facilities. Additionally, as Wangler et al. [10] stated, the RTD must be known to further develop and scale up the newly developed manufacturing methods.

Since the RTD is often hard to model, tracer experiments were developed to measure the RTD [15, 16]. With this experiment, a tracer material is injected at some location into the system and detected at another location, which is usually the outlet of the system. The RTD can be calculated as the frequency density distribution of the time between injection and detection. The traceability of a material depends on the material that is carrying it and the suitability of injection and detection devices. Since this depends on the process in which it is applied, it is not self-evident that existing tracer experiments can be applied to other materials and processes. Therefore, the concrete industry must develop suitable tracer experiments for their processes.

To the authors' knowledge, only two tracer experiments have been developed for concrete processing. First, Heller [17] developed a radiotracer technique, with which specific elements of the material can be either marked with radioactive material or activated themselves. This method can trace the material components individually at a high sample rate. Furthermore, the tracer can be detected through obstructions if the radioactivity is sufficiently high. Second, Wangler et al. [14] applied a pigment suspension of chromium oxide as the tracer material and detected it offline by EDX analysis on samples from the product. This offline method is labor-intensive and has a relatively low sample rate (~0.02 Hz). Even though the method has functioned, it can still be improved by performing it in-line. An in-line method can increase the sample rate significantly without requiring intensive labor. The high sample rate is important when the variance of the residence time is low and/or the mean residence time is short. Besides, a non-labor-intensive method combined with easy-to-implement low-cost equipment is more likely to be widely adopted. It will enhance the comparison between different material-system combinations and the integration into automated workflows for quality and process control [18].

This paper introduces an in-line dye tracer experiment using a digital image processing (DIP) technique. With this experiment, we aim to overcome the thresholds for adopting tracer experiments for concrete processing. These thresholds are per-sample cost, availability and cost of equipment, and ease and speed of implementation. Most thresholds can be overcome by detecting the tracer dye in-line with a high sample rate using a low-cost industrial camera. We acknowledge that the presented method has some drawbacks, such as the need for homogenization of the filament before detection and that it is mainly the water within the material that is traced rather than the particles.

In the following section, the different residence functions and properties are summarized. In section three, we describe how to apply and detect the dye used as tracer material, focusing primarily on the in-line measurement system that collects and processes digital images in real time. The noise reduction measures are described in detail since these influence the amount of tracer material needed. In the fourth section, the results are presented and discussed. First, the signal-to-noise ratio of different color values is presented, followed by the correlation between the tracer concentration and the measured color intensity. Finally, the tracer experiment is validated on a 3DCP system by obtaining the residence time functions from impulse, step-up and step-down inputs for different tracer quantities. In section five, the main findings of this study are summarized, and recommendations for further development are discussed. In the final section, an outlook outlines recommended RTD properties for reporting, intended for enhancing the comparison of various material-system combinations.

2 Residence time theory

2.1 Residence time functions

Three functions commonly present the residence time [19, 20]. First, the RTD or frequency function $E(t)$ is the frequency density distribution of residence time. The RTD can directly be obtained from a tracer experiment by measuring the response to an impulse input that is applied at $t = 0$ and is calculated as

$$E(t) = \frac{C(t)}{\int_0^\infty C(t)\,dt} \approx \frac{C(t_i)}{\sum_{i=1}^{n} C(t_i)\,\Delta t_i}, \tag{1}$$

where $C(t)$ is the tracer concentration at time t. As for any frequency density distribution, the area underneath the RTD equals one. Second, the cumulative residence time function $F(t)$, which can be experimentally determined by measuring the response to a step-up input and is calculated as

$$F(t) = \int_0^t E(t)\,dt \approx \sum_{i=1}^{n} E(t_i)\,\Delta t_i. \tag{2}$$

This function has the properties $\lim_{t\to-\infty} F(t) = 0$ and $\lim_{t\to\infty} F(t) = 1$. Third, the wash-out function $W(t)$ is the response to a step-down input and is expressed as

$$W(t) = 1 - F(t). \tag{3}$$

As shown in the equations above, all representations can be readily derived from one another by integration and derivation. Converting these equations is only valid if the examined combination of system and material is linear time-invariant, meaning it has a steady flow that does not change over time. The most common method to obtain the RTD is injecting the tracer material with an impulse input and, to a lesser extent, with a step input. Impulse inputs are generally preferred since the smooth curves obtained from step inputs can hide real effects [16]. However, for specific systems with, for instance, highly pressurized injection ports, it is not practical to apply a perfect impulse input. The current research compares the three types of inputs to validate the tracer experiment.

2.2 Residence time properties

The RTD has several properties that this research compares. The first property is the mean residence time $\bar{t}$ and is calculated as

$$\bar{t} = \int_0^\infty t\,E(t)\,dt \approx \sum_{i=1}^{n} t_i\,E(t_i)\,\Delta t_i. \tag{4}$$

The mean residence time is equal to V/Q where V is the volume of the system and Q the volumetric flow rate of the material. Deviations from the mean can indicate that a dead zone is present in the system, which changes the effective volume.

The second property, the spread of the residence time, is obtained from calculating the second moment around the mean and is indicated as the mean-centered variance σ^2 of the frequency function

$$\sigma^2 = \int_0^\infty \left(t - \bar{t}\right)^2 E(t)\,dt \approx \sum_{i=1}^{n} t_i^2\,E(t_i)\,\Delta t_i - \bar{t}^2. \tag{5}$$

The mean-centered variance can be made dimensionless as $\overline{\sigma}^2 = \sigma^2/\bar{t}^2$. The variance σ^2 is an indicator of the spread of the residence time distribution. Furthermore, a higher variance means that dosing fluctuations will be damped more over time, which is preferable for achieving temporal homogeneity. For example, an ideal continuous stirred-tank reactor (CSTR) has a dimensionless variance $\overline{\sigma}^2$ equal to one, while a plug flow reactor (PFR) has a dimensionless variance $\overline{\sigma}^2$ equal to zero.

The mean residence time $\bar{t}$ and mean-centered variance σ^2 can also be obtained from a step-up response as

$$\bar{t} = \frac{\int_0^\infty C_{\max} - C(t)\,dt}{C_{\max}} \approx \frac{\sum_{i=1}^{n} \left(C_{\max} - C(t_i)\right)\Delta t_i}{C_{\max}} \tag{6}$$

and

$$\sigma^2 = \frac{2\int_0^\infty t\left(C_{\max} - C(t)\right)dt}{C_{\max}} - \bar{t}^2 \approx \frac{2\sum_{i=1}^{n} t_i\left(C_{\max} - C(t_i)\right)\Delta t_i}{C_{\max}} - \bar{t}^2 \tag{7}$$

where C_{max} is the maximum tracer concentration. When the response to a step input is normalized ($C_{max} = 1$), the Eqs. (6) and (7) can be simplified, resulting

$$\bar{t} = \int_0^\infty 1 - F(t)\,dt \approx \sum_{i=1}^{n} \left(1 - F\left(t_i\right)\right) \Delta t_i \tag{8}$$

and

$$\begin{aligned} \sigma^2 &= 2 \int_0^\infty t\,(1 - F(t))\,dt - \bar{t}^2 \\ &\approx 2 \sum_{i=1}^{n} \left(t_i \left(1 - F\left(t_i\right)\right) \Delta t_i\right) - \bar{t}^2. \end{aligned} \tag{9}$$

The mean residence time $\bar{t}$ and mean-centered variance σ^2 can be obtained directly from the cumulative residence time function $F(t)$ and the wash-out function $W(t)$ since $W(t) = 1 - F(t)$.

The third property is the percentiles of the RTD. The percentiles can be read directly from the cumulative residence time graph and indicate when a certain percentage of the tracer material left the system. When the RTD has a long tail and is highly skewed, the percentiles, such as the median (50th percentile), give a more representative value than the mean and the variance since a long tail can pull away the mean from the median. Additionally, the percentiles give a more practical representation from a process control engineering perspective. For example, the 99th percentile indicates the time needed to reach 99% of the change in properties after adjusting an input flow. Therefore, process control engineers usually prefer step inputs over impulse inputs.

3 Materials and methods

3.1 The 3DCP system and material

The 3D concrete printing system at the Structures Lab of Eindhoven University of Technology was used with the Weber 3D 145–2 mix [12] as a bulk material to validate the tracer experiment. This bulk material is a premix composed of Portland cement, siliceous aggregates with a maximum particle size of 1 mm, limestone fillers, specific additives, and a small number of polypropylene fibers. To obtain a printable mortar, 15% ± 0.5% water was added by weight. Figure 1 shows the printing system consisting of an

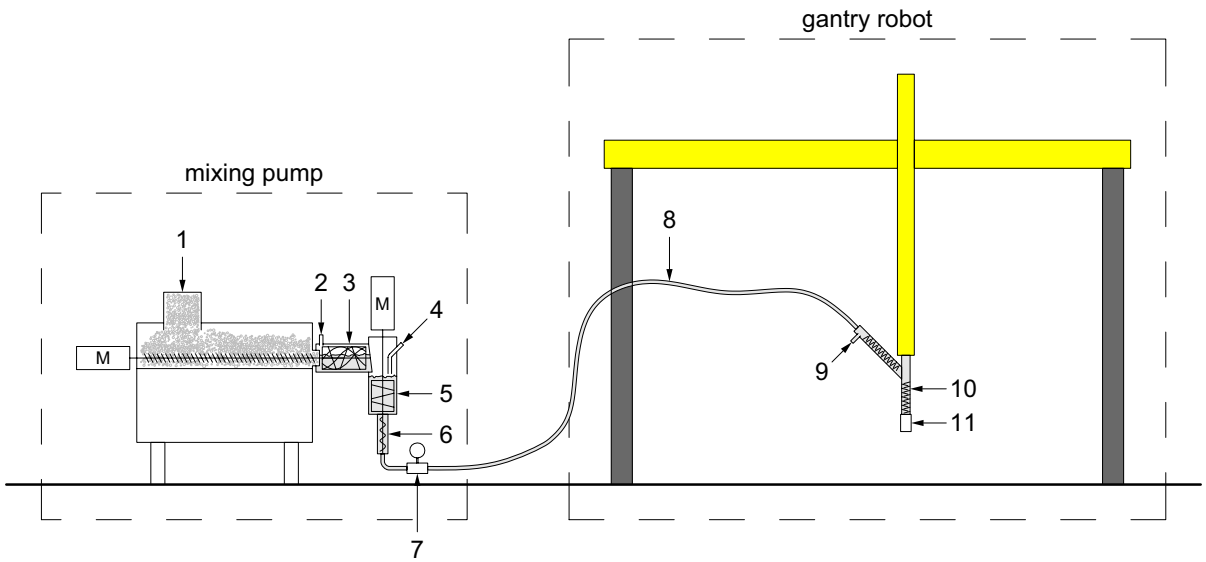

Fig. 1 Schematic overview of the 3D concrete printing system with the mixing pump and gantry robot. (1) Inlet for the dry premix. (2) Water inlet. (3) Horizontal mixing chamber. (4) Tracer injection port A. (5) Vertical mixing chamber. (6) Progressive cavity pump. (7) Mortar pressure sensor. (8) 10 m-long hose. (9) Tracer injection port B. (10) Helical static mixing elements. (11) Nozzle with the detection device (see Fig. 2)

M-tec duo-mix connect for mixing and conveying the cement-based mortar, a 10 m-long hose with an inner diameter of 25 mm to transport the material to a rectangular nozzle and a gantry robot. The mixing pump mixes the powders and liquids in two stages. First, the mixing pump mixes a batch of dry premixed material with water in the horizontal mixing chamber. The material is transported in batches from this mixing chamber to the second vertical mixing chamber. From here, the system transports the wet mortar with a progressive cavity pump. For our experiments, the frequency of the progressive cavity pump (D4−¼ with an integrated clamp) was set to approximately 210 RPM and fixed for all experiments. For this process parameter, the dosing time of each batch was approximately 5 s and the mean time interval between batches was approximately 15–20 s. The material was continuously mixed in the second mixing chamber and pumped with a mean mass flow rate of 6.5 kg/min and a mean volume flow rate of around 3 L/min. The mass flow rate of the mortar varied between and within print sessions. Therefore, the actual mass flow was measured manually at regular intervals during all experiments and reported in the results section.

3.2 Selection of the tracer material

For the selection of the tracer material, there are two requirements. First, the tracer material has to be detectable from the bulk material, which means the signal-to-noise ratio (SNR) should be maximized. Second, the tracer material should have a minimal influence on the properties of the bulk material, since a change in properties can affect the flow behavior of the material and thus the residence time distribution. Therefore, the tracer material should not react with the bulk material or decay inside the examined system. The tracer material cannot be selected independently from the measurement device since the noise the detection device introduces significantly influences the SNR. As tracer material, a color dye was selected because of the ease of implementation since it detects the tracer material with relatively simple equipment. Besides that, the used mortar has a relatively light grey color, which makes it a suitable mortar to stain with a color dye. The dye Rhodamine B (RhB) was selected since it fulfills these requirements. RhB is a well-known tracer dye, visible and thus detectable, even in low quantities. In addition, RhB does not influence the mechanical properties of the bulk material since it does not react with cement-based materials and has negligible sensitivity to the alkalinity of cement-based materials [21]. However, RhB, an organic dye, degrades when exposed to ultraviolet (UV) light. Since the tracer material was measured in-line within several minutes after injection, this decay is assumed to be negligible. The disadvantage of RhB is that, because of safety reasons and to be able to dose the tracer material accurately, it had to be dissolved in water, which resulted in a change in the water-to-solids percentage of the mortar due to the addition of the tracer. Therefore, the highest dissolvable concentration of 15 g RhB per liter of distilled water was used to influence the material properties as little as possible. Note that, in this paper, the reported quantities of tracer material are for the RhB solution, not the amount of RhB powder.

3.3 Injecting the tracer material

The tracer material was injected at injection port A (Fig. 1) into the second mixing chamber of the mixing pump. Impulses were applied with syringes that were manually emptied into the mixing chamber. The tracer material was injected within the 5 s interval in which the bulk material was added to the second mixing chamber. Additionally, the tracer material was applied with step-up and step-down inputs. Between the step changes, the tracer material was constantly dosed for approximately 8 min to achieve a bulk material with a stable tracer quantity at the system outlet. The start of a step change was manually aligned with the start of the 5 s interval in which a batch with bulk material was added to the mixing chamber. The step inputs were applied with a dosing system consisting of a gear pump (Tuthill D-series) and a Coriolis mass flow sensor (Bronkhorst MI140). A gear pump was selected since it doses the tracer material with minimal pulsation and, thus, with a relatively constant flow. The mass flow sensor was selected because of its low zero stability of 0.1 g/min and high reading accuracy of $\pm 0.2\%$. The system used had an integrated PI controller that adjusted the frequency of the gear pump based on the set mass flow rate. The mass flow rate of the tracer material was adjusted and logged with a sample rate of 0.1 s with the Bronkhorst Flow Suite software package.

The tracer material was dosed from a tank and constantly mixed with a magnetic stirrer.

The quantity of the tracer material was varied to study if the tracer quantity influences the residence time functions. Based on exploratory experiments, impulse sizes of 15, 30 and 60 g and step changes of 15, 30 and 60 g/min were chosen. To avoid system failures, such as blockage of the injection ports, and to have a better response of the used dosing system, there was always a minimum flow of tracer material of 5 gr/min through the injection line. This minimum flow resulted in step changes of 5 to 25, 5 to 35, 5 to 65 and vice versa. For each tracer quantity, the experiment was performed three times.

3.4 Detecting the tracer material

There were three requirements for detecting the tracer material. First, since RhB was used as a color dye, the color intensity had to be measured with a high SNR. Second, the sample rate needed to be sufficient to measure the system's behavior without missing any fast dynamics. Third, the measurement needed to be performed in-line to have a non-labor-intensive method, which also benefits the second requirement to obtain a high sample rate. Other studies showed that these requirements can be fulfilled by measuring the color intensity with spectrometers that operate in the visible light spectrum [22, 23]. As an alternative, digital image processing (DIP) techniques were used to obtain the color intensity from digital images [24–26]. To have a cost-effective solution and since the amount of tracer material was measured in a wet and dirty environment, a more robust industrial camera in combination with a white LED light source was used instead of a more expensive spectrometer. Both these methods measure the color intensity of the material's surface. Here, the local tracer content can vary from the average due to particle migration and convection [27, 28]. To ensure that these surface measurements reflect the average tracer content, the material was homogenized just before detection by placing 25 helical static mixing elements (2×PRIMIX PMS25-10-316L-CHAIN and 1×PMS25-5-316L-CHAIN) with a total length of 1065 mm before the nozzle.

The DIP technique was implemented as follows. The industrial camera (Basler a2A1920-51gcPRO) and the light source (PL-ELSB-105SW) with a color temperature of 5500 K ± 500 K were mounted at the printhead of the 3D concrete printer, as shown in Fig. 2. The camera was mounted above the nozzle with an outlet of 50 × 10 mm^2. For practical reasons, such as waste disposal and wiring, a nozzle with a slide was used to keep the gantry robot in a stationary position. The slide had a short horizontal part where the camera was focused at. The distance between the filament surface and the lens (Edmund Optics 16MM Compact Fixed Focal Length) was approximately 100 mm. Via the software Vision Builder AI from National Instruments, images of the mortar surface were acquired. In real-time, the average linear RGB color value was obtained from a region of interest (ROI) of 850 by 300 pixels, approximately 23 by 7 mm^2, with a sample rate of 15 samples per second. One of the hundred images was saved to have a visual check afterward. Figure 3 shows typically acquired images with the ROI. Theoretically, it is possible to obtain higher sample rates by analyzing the images (or video) after the experiment since the real-time calculation of the average color value decreased the sample rate. However, the lower sample rate was sufficient for the presented study.

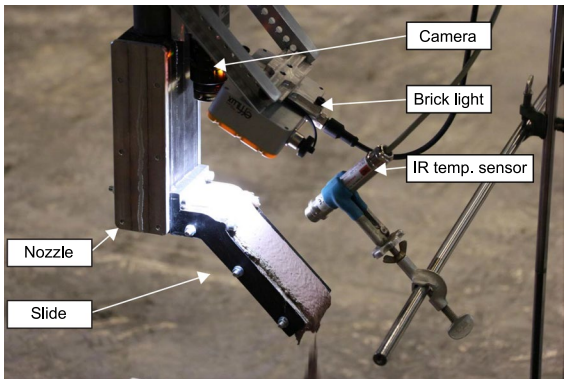

Fig. 2 Polarized camera, polarized brick light, IR temperature sensor and nozzle with slide mounted at the printhead

3.5 Noise reduction measures

Various settings and options significantly influence the measurement noise within the presented DIP method. Reducing noise was a crucial parameter in improving the SNR since, for increasing the signal, unwanted higher quantities of tracer material are needed that influence the bulk material's properties.

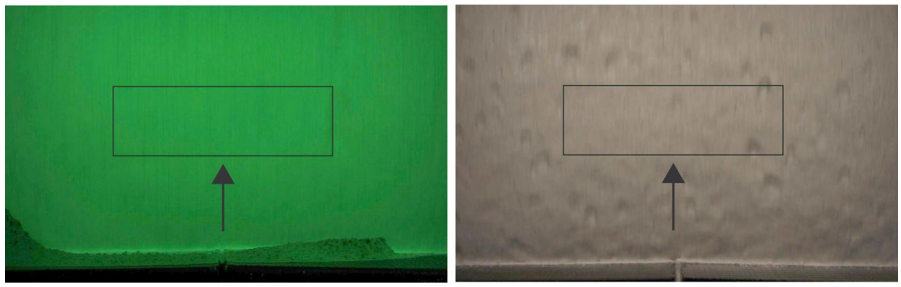

Fig. 3 Acquired images with the region of interest indicated by a dark grey rectangular box and the flow direction of the mortar indicated by a dark grey arrow. The left image was acquired using a bandpass filter, and the right image without a bandpass filter

Therefore, the various settings and choices made within the presented DIP technique that influence the measurement noise are discussed in detail in the following paragraphs.

Sources of noise in digital image measurements are glare and shadows, respectively, causing light and dark spots in the image. The glare was the primary source of measurement noise to reduce since the wet surface of fresh mortars is reflective. A single polarized light source in combination with a polarization filter on the lens or a diffuse light source prevents glare. Even though diffuse light reduces dark shadows, a single polarized brick light (PL-ELSB-105SW) was combined with a linear polarization filter (Midwest Optical PR032-25.5). This choice was made because, with a diffuse omnidirectional light source, for example, a dome light, the nozzle partly blocks the light source, making it impossible to create a diffuse light on the measured surface. Additionally, with a more compact brick light, the industrial camera could be placed closer to the nozzle outlet. When the slide is removed from the nozzle, it is possible to use the presented implementation in an actual print session since the camera is focused on the filament as close as possible to the nozzle outlet. The brick light was placed, at best, in parallel with the orientation of the lens to minimize dark shadows.

Even though a spectrometer acquires data over the entire visible light spectrum, it is a common technique to determine the amount of tracer material from a light spectrum by only considering the light absorbance at a specific wavelength, usually where the highest intensity difference is measured. This approach can be mimicked with an industrial camera by mounting a bandpass filter on the lens that only transmits a small bandwidth of the light spectrum. The absorption excitation wavelength of RhB lies approximately between 545 and 560 nm [29]. Therefore, a bandpass filter (Midwest Optical Bi550) with a narrow bandwidth of approximately 535 to 558 nm that closely matches the excitation range of RhB was selected. Since narrow bandpass filters block most of the light spectrum, the hypothesis is that this approach will reduce measurement noise since only the excitation wavelengths are considered and the noise from the wavelengths that are not of interest is neglected. We compared the use of the bandpass filter with unfiltered data for different quantities of tracer material in the first part of the results section. For the case without a bandpass filter, a UV protection filter (Midwest Optical AC400) was used instead of a bandpass filter.

3.6 Camera calibration procedure

An industrial camera has a variety of settings available. An 18% grey card was used to determine the settings and calibrate the detection device before every experiment. The calibration procedure improves the experiment's repeatability. The grey card's linear RGB color values are 18%, considering 0% black and 100% pure white. The calibration procedure was as follows. First, all settings of the industrial camera were set to manual to eliminate automatic corrections during the experiments. Second, measurements of several hours on the 18% grey card showed that the measured color reached a stable value after 50 min of data acquisition. Therefore, the camera and light source were enabled for at least one hour before the calibration procedure and experiment. Third, the white balance ratio was adjusted to have equal linear RGB color values. Fourth, the light intensity was scaled to obtain linear RGB color values of 18%. The light intensity, the amount of light transmitted to the camera's sensor, depends on three parameters: the exposure time, gain level and aperture of the lens, the latter indicated by the Fstop number. The three parameters are related to each other. For example,

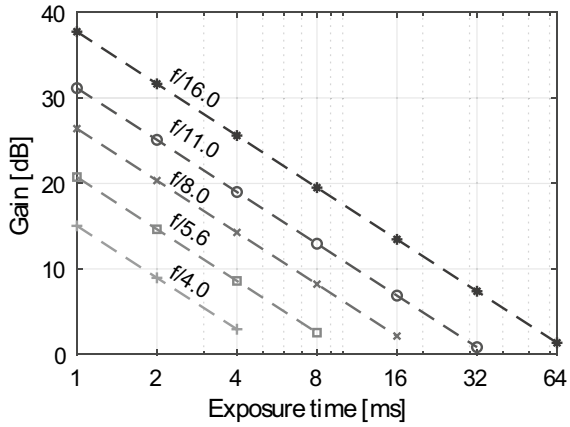

Fig. 4 Relation between the exposure time and gain level for different apertures to obtain an 18% grey color without a bandpass filter

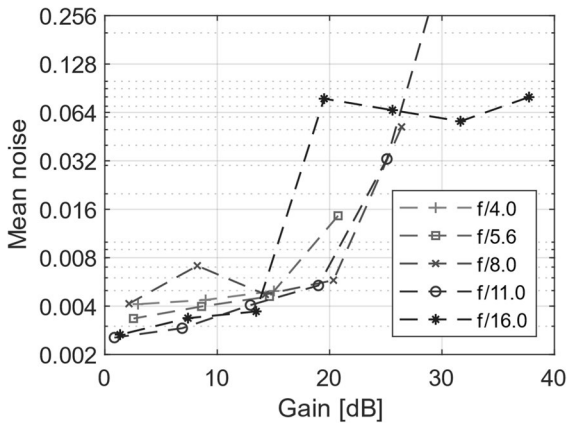

Fig. 5 Relation between the gain level and mean measurement noise for different apertures to obtain an 18% grey color without a bandpass filter

when the lens's aperture increases, the exposure time or the digital gain level needs to be decreased to get the same color intensity. To find the optimal settings with a high SNR, 3-min measurements on the 18% grey card were performed for different exposure times and lens aperture combinations. The gain level was adjusted for each combination to reach the linear RGB color values of 18%. Figure 4 shows the values and relationships between the tested parameters.

The measurement noise for each 3 min measurement was calculated to decide the optimal combination of parameters. The average color distance to the average color in CIELAB color space was used as the value for the measurement noise. Figure 5 shows the measured noise versus the required gain level and reveals a tipping point at a gain level of 20 dB. To stay below the tipping point of 20 dB, lower Fstop numbers and higher exposure times are required, resulting in a smaller depth of view and an increase in motion blur. However, these effects are less interesting than the measurement noise since only the color value was of interest and not the image sharpness. Therefore, a low gain level was chosen for all experiments. For all measurements, an aperture of f/8 was selected. For the use with a bandpass filter, the exposure time was set to 64 ms; without a bandpass filter, the exposure time was set to 16 ms. These settings resulted in gain levels of approximately 5 and 2.5 dB, respectively. The gain levels slightly differed in each experiment since small unintentional changes such as the position of the light source, camera and the polarization filter influence the light intensity. Since a bandpass filter transmits less light, a longer exposure time and a slightly higher gain level were needed compared to unfiltered measurements.

As the last step of the calibration procedure, the white reference point was determined by using a white balance card and measuring the XYZ values in CIEXYZ color space with National Vision Builder AI. The white reference point was used to transform the obtained data from the linear RGB color space to the CIELAB color space. An additional step was needed if a bandpass filter was used since most of the visible light spectrum was blocked. Applying the bandpass filter resulted in an excitation of the green color value and thus, the linear RGB color values could not be equally scaled to 18%. Therefore, the described procedure without a bandpass filter was used first to balance the color values. After that, the bandpass filter was mounted on the lens and the gain level was adjusted. As an alternative to scaling the linear RGB color values, the light intensity L* of the CIELAB color space was set to 50% by adjusting the gain level, corresponding to the L* value of an 18% gray card.

Although the noise caused by the measurement device was minimized on measurements of the assumed uniformly colored and flat surface of an 18% grey card, additional parameters influenced the noise. For instance, the bulk material can have color

fluctuations and cavities can introduce dark shadows (even if it was prevented at best). Therefore, the first part of the research aims to quantify the detectability of the tracer material by calculating the total SNR for different tracer quantities.

3.7 Calibration curve

The correlation between the different tracer concentrations and the measured color value needs to be known to estimate the amount of tracer material in the bulk material. There are two methods. First, calibration curves can be fitted between the color intensity and various tracer concentrations. Second, the correlation between the impulse sizes and the area underneath the graph of the color value after applying a baseline correction can prove linearity [25]. Here, the different impulses of 15, 30 and 60 g were used. The advantage of the second method is that there is no need for a dosing system. However, this method is only suitable if the correlation between the tracer concentration and the measured color value is linear. If there is no linear relation, a calibration curve is still needed.

The tracer quantities for defining the SNR and the calibration curve were decided by applying six intervals between the minimum (5 g/min) and maximum mass flow rate of the three different step sizes (20, 35 and 65 g/min). Applying the intervals in combination with the desired minimum and maximum mass flow rates resulted in the following three sets, {5, 7.5,10, 12.5, 15, 17.5, 20}, {5, 10, 15, 20, 25, 30, 35} and {5, 15, 25, 35, 45, 55, 65}. The dosing quantities of the three individual sets were combined in one set, namely, {5, 7.5,10, 12.5, 15, 17.5, 20, 25, 30, 35, 45, 55, 65}, that was shuffled in random order four times and injected at injection port B (Fig. 1) into the printhead within one print session. The different quantities of tracer material were injected at the end of the hose, just before the static mixing elements at the printhead. The RhB was continuously injected for 3 min for each mass flow rate. Even though a printhead with static mixing elements can be expected to behave near a plug-flow reactor with minimum damping, the dosing system used needs 10 to 20 s to reach a stable value. Therefore, one minute from the sampled data was used for analysis to ensure no other system behavior was captured in the analyzed data. The different quantities of tracer material were continuously injected with the earlier described dosing system. The experiment was performed with and without the use of the bandpass filter.

3.8 Statistical and data analysis

Linear RGB color values are obtained as the mean of the region of interest for every captured frame. The linear RGB color values were transposed to CIELAB color space to compare their detectability. The main difference between the two color spaces is that the CIELAB color space intends to be perceptually uniform. Therefore, this color space is commonly used to indicate color differences through the Euclidean distance between two colors. The SNR, the ratio between the mean and standard deviation, quantifies the detectability. A Hampel filter was applied once to remove outliers for both color spaces. A window size of 15 neighbors was used for either side of the data point. An outlier was removed if the R, G, B, L*, a* or b* value of that data point was more than six scaled median absolute deviations away from the median. Afterward, the color values were filtered by applying a moving mean with a total window size of 15 samples. Since the window size is approximately one second, the data still gives sufficient detail with an accuracy of one second.

The distance between single color values was calculated by subtracting a reference value, which was found by fitting a linear curve through the obtained color values. On this curve, the reference point was placed at an Euclidian color distance of three from the average color value at a tracer mass flow rate of 5 g/min. For each printing session, the reference point was re-calculated. The Euclidian color distances were calculated from the single-color distances as

$$d(R,G,B) = \sqrt{\Delta R^2 + \Delta G^2 + \Delta B^2}, \tag{10}$$

$$d(a^*,b^*) = \sqrt{\Delta a^{*2} + \Delta b^{*2}}, \tag{11}$$

$$d(L^*,a^*,b^*) = \sqrt{\Delta L^{*2} + \Delta a^{*2} + \Delta b^{*2}}. \tag{12}$$

A baseline correction was performed with the average color distance for a tracer mass flow rate

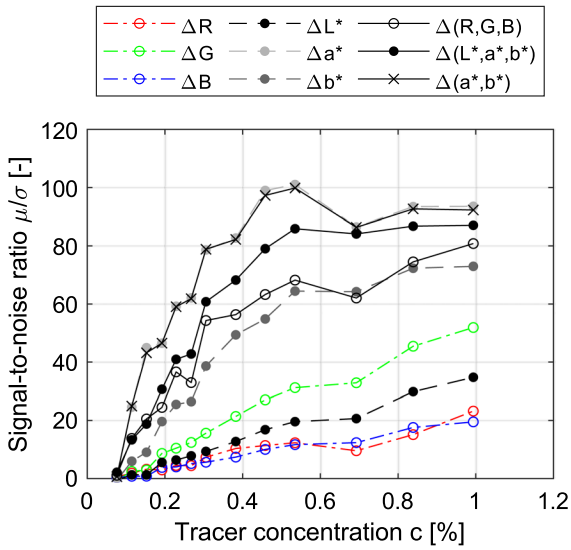

Fig. 6 SNR as a function of tracer concentration for various color distances without a bandpass filter

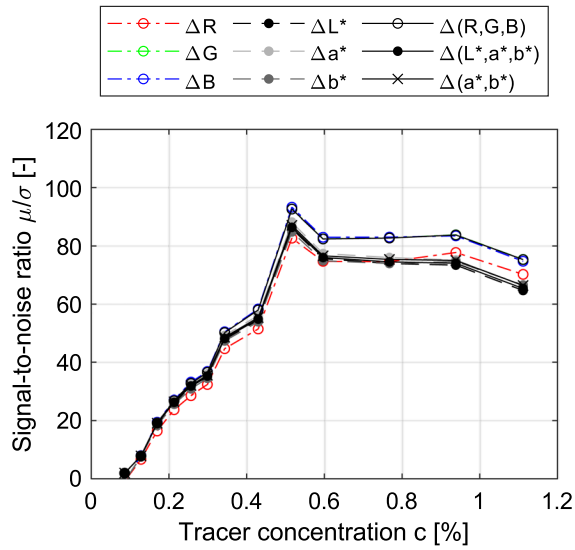

Fig. 7 Using a bandpass filter, SNR as a function of tracer concentration for various color distances

of 5 g/min. For the step responses, the average color value of the upper concentration was used for normalization.

3.9 Data acquisition of other process values

Overall process parameters of the 3D concrete printing system, such as the pump frequency, mortar pressure and water dosing for the bulk material, were logged via the software package Node-RED on a desktop computer. The M-tec duo mix connect and the SINUMERIK controller of the gantry robot were connected to this desktop computer and data were transferred via the OPC UA protocol. Besides that, a separate measurement system with a contactless infrared temperature sensor was used to measure the temperature of the mortar when it exits the nozzle. The data from the various log files were matched based on the timestamps. The data matching and analysis were performed in the MATLAB (Mathworks) programming environment.

4 Results and discussion

4.1 Detectability of the tracer

Two print sessions were executed, with and without a bandpass filter, each taking approximately three hours. During the first session, the mass flow rate decreased linearly from approximately 6.9 to 6.2 kg/min; during the second session, the flow rate decreased linearly from approximately 6.4 to 5.4 kg/min. This decrease is equivalent to a linear decrease of 0.23 and 0.30 kg/h, respectively. The most likely cause for the decrease in flow rate is the wear of the rotor–stator pump. However, further research is required since not all observations have been explained yet. Variations between print sessions can be attributed to the manual reassembly of the rotor–stator before each session since the tightness of the clamps directly influences the material output. The temperature was around 30 °C and within a range of ± 1 °C for all print sessions. Even though the color value of RhB is influenced by the temperature [30], the temperature was not considered in the analysis since it was stable. This might differ from systems with high-temperature development or fluctuations within or between print sessions.

4.2 Detectability of the tracer: signal-to-noise ratio

Figures 6 and 7 show the filtered (with a bandpass filter) and unfiltered SNR as a function of tracer concentrations for various color distances. There were, in total, 25 outliers removed from the two datasets. Both figures show that the SNR increases with increasing tracer concentration, except for the unfiltered distances Δa^* and $\Delta(a^*, b^*)$. Furthermore, all filtered results have a maximum SNR at a tracer concentration of 0.5%, after which a plateau is reached. The SNR of the filtered (Fig. 7) color distances are similar for equal tracer concentrations, while for the unfiltered results (Fig. 6) the choice of color difference significantly impacts the SNR. Here, the SNR of the color distances in the CIELAB color space is higher than the RGB color space. Using a bandpass filter flattens the results, significantly improving the distances with low SNR and slightly worsening the high SNR compared to the unfiltered results.

The conclusion is that the chroma plane color distance $\Delta(a^*, b^*)$ in the CIELAB color space without a bandpass filter gives the highest SNR and, therefore, will be used for further experiments. The highest SNR is reached at a tracer concentration of 0.5%. Therefore, tracer concentrations above 0.5% have no added benefit. Wahl et. Al. [26] also compared different color spaces for the data gathered from their tracer experiment and concluded that the CIELAB color space gave the best results. Besides that, the CIELAB color space was also used in other tracer studies that used digital images [16, 17]. However, these studies did not compare different color spaces.

4.3 Detectability of the tracer: correlation

Figure 8 shows the calibration curve, the correlation between the tracer concentration and the color distance $\Delta(a^*, b^*)$. Considering the whole dataset, the correlation between the tracer concentration and the color distance is a second-order polynomial. The tracer concentration is estimated with the following linear regression model:

$$\tilde{c} = \Big(0.68\,\Delta(a^*, b^*)^2 + 13.70\,\Delta(a^*, b^*) + 7.07\Big)10^{-4} \tag{13}$$

where $\tilde{c}$ is the estimated tracer concentration. In the lower regions, with tracer concentrations up to 0.4%, the correlation can be assumed to be linear and is estimated with

$$\tilde{c} = (14.53\,\Delta(a^*, b^*) + 7.08)10^{-4}. \tag{14}$$

Both regression models have an adjusted R-squared of 0.98. Up to a concentration of 0.4%, the calibration curve only scales the output curve but does not change its shape. Therefore, the RTD can be identified without applying the calibration curve. The calibration curve should be used if concentrations above the Limit of Linearity (LOL) are applied. The correlation between the impulse sizes and the area underneath the color distance $\Delta(a^*, b^*)$

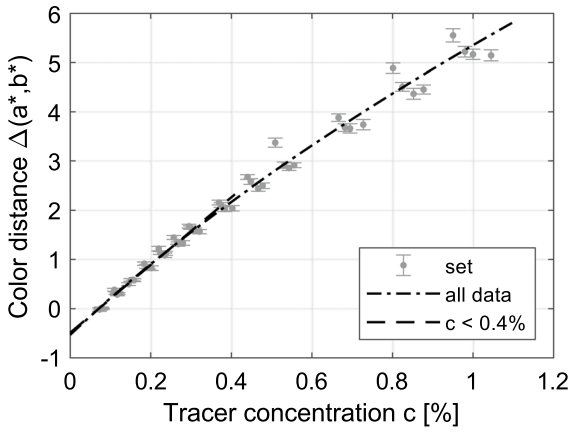

Fig. 8 The correlation between the chroma color distance and the tracer concentration. The error bars represent ± two times the standard deviation

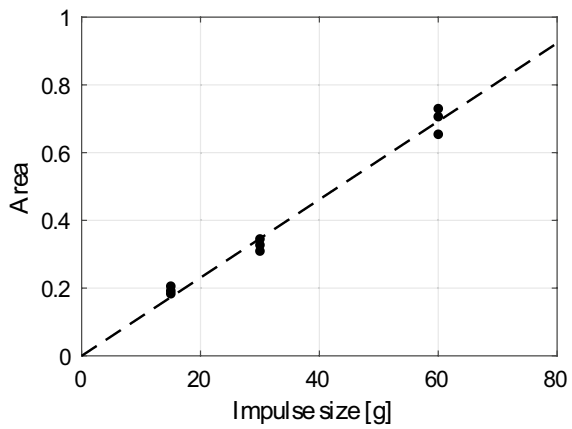

Fig. 9 The correlation between the impulse sizes and the area under the color distance curve

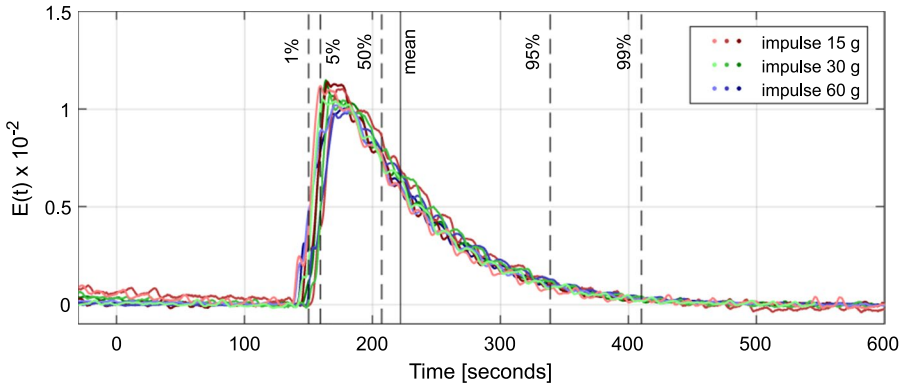

Fig. 10 Residence time distributions obtained from impulse inputs for impulse sizes of 15 g (three red shades), 30 g (three green shades) and 60 g (three blue shades). The vertical dashed lines indicate the average percentiles and the vertical solid line represents the average mean of the nine experiments

graph also indicates the lower concentrations' linearity. Figure 9 shows that the area underneath the color distance curve is proportional to the impulse size, with an adjusted R-squared of 0.98. Using Eq. (13) as an estimator, the maximum tracer concentration from the impulse inputs is 0.8%.

As a result of the impulse inputs, the maximum obtained tracer concentration is 0.8%. The calibration curve suggests that the relation is not strictly linear at these higher tracer concentrations. However, these tracer concentrations only occurred at the peak of the RTD and thus for a short period (see Fig. 10). Therefore, it only represents a part of the area under the curve. This short duration might explain why there is still a robust linear relationship. It is recommended to prove linearity with impulse sizes higher than the intended impulse size used to determine the RTD. For the examined system and material, the impulse size to prove linearity should be twice as high as the impulse size to obtain the RTD.

4.4 Comparison of input types

The responses to the step-up, step-down and impulse inputs were obtained within one print session. The frequency of the pump was around 204 RPM. The mortar mass flow rate decreased approximately from 6.2 kg/min to 5.6 kg/min during the first two and half hours; whereafter it increased to 6.1 kg/min. The entire session took around four hours, wherein the mortar temperature fluctuated between 28.5 and 30.5 °C. From the obtained dataset with roughly 210.000 samples, 29 outliers were removed. The color distances $\Delta(a^*, b^*)$ were calculated as explained in Sect. 2, where the tracer concentrations were then estimated with the linear regression model in Eq. (13).

Figure 10, 11 and 12 show the RTD, normalized step-up and normalized step-down responses. The data in these graphs were obtained as follows. First, a baseline correction was applied since the minimum tracer mass flow rate was 5 g/min. Second, the RTD was calculated by using Eq. (1) for the impulse inputs. The average tracer concentration of

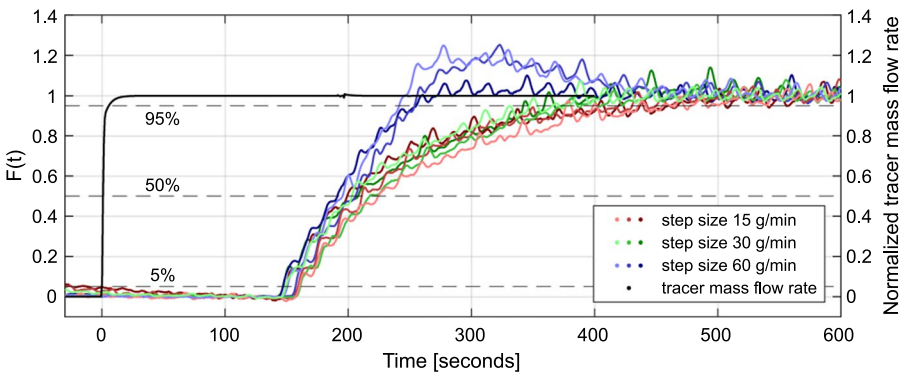

Fig. 11 Cumulative residence time functions obtained from step-up inputs for step sizes of 15 g/min (three red shades), 30 g/min (three green shades) and 60 g/min (three blue shades). The horizontal dashed lines indicate the percentiles

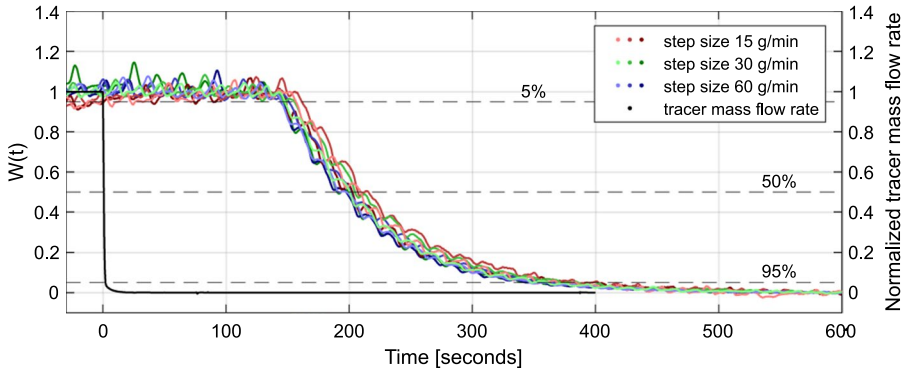

Fig. 12 Wash-out function obtained from step-down inputs for step sizes of 15 g/min (three red shades), 30 g/min (three green shades) and 60 g/min (three blue shades). The horizontal dashed lines indicate the percentiles

each response between 100 to 130 and 570 to 600 s was used for the baseline correction and normalization of the step responses. The data before 100 s was not used since the tracer concentration was not stable in this region. In some cases, an apparent, stable plateau was not reached within the 8-min interval between step changes and impulse inputs.

The RTD, shown in Fig. 10, is similar for different impulse sizes. After applying the impulses, there is a dead time of 130 to 140 s, whereafter, there is a steep increase with a peak between 150 and 200 s followed by a decay that ends around 500 s. Figure 11 shows the normalized step-up responses, representing the experimentally determined cumulative residence time function $F(t)$. Here, all examined step sizes have a dead time of 130 to 140 s. However, the shape of the step responses after 140 s differs for the largest examined step size of 60 g/min. The tracer concentration increases faster for this step size than the two lower examined step sizes. Two of the three experiments have an overshoot before reaching a stable plateau after approximately 500 s. Figure 12 shows the step-down responses that represent the experimentally determined wash-out function $W(t)$. Here, the graphs show a similar trend for all examined step sizes. First, there is a dead time of 130–140 s, whereafter, there is decay that ends around 500 s. The graph shows a wavy pattern with roughly 15 to 20 s intervals for all presented data.

The maximum estimated tracer concentrations from the three impulse sizes are approximately 0.3%, 0.45% and 0.8%. The maximum estimated tracer concentrations for the three different step sizes are 0.4%, 0.8% and 1.6%. With a mortar mass flow rate of 6 kg/min and a water-to-solids percentage of 15% by weight (including the 5 g/min of tracer material)

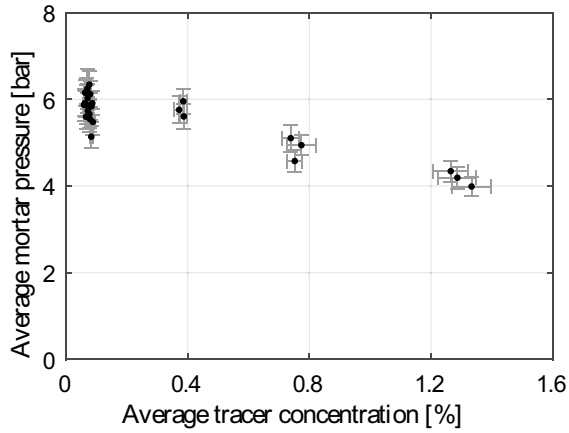

Fig. 13 The average tracer concentration versus the average mortar pumping pressure. The values were obtained by taking the average values from the stable plateaus between the impulse and step inputs. The error bars represent +/− two times the standard deviation

for the original process, the water-to-solids percentage increased from 15% to approximately a maximum of 15.25%, 15.45% and 15.85% for the three different impulse sizes, while for the step responses to a maximum of approximately 15.40%, 15.85% and 16.75% due to the addition of tracer material. Additionally, Fig. 13 shows the relationship between the tracer concentration and the mortar pumping pressure. The average tracer concentration and pressure shown were obtained from the stable plateaus of one minute between the impulse and step inputs. The figure shows that the pumping pressure is around 6 bar for the original process, while for higher tracer concentrations, the pumping pressure decreases to 4 bar.

Table 1 shows the mean residence times $\bar{t}$ and standard deviations σ obtained with Eqs. (4) till (9).

Table 1 The residence properties obtained from the various impulse, step-up and step-down inputs for different tracer quantities

	Experiment 1			Experiment 2			Experiment 3		
	$\bar{t}$ [s]	σ [s]	$\bar{\sigma}^2$ [−]	$\bar{t}$ [s]	σ [s]	$\bar{\sigma}^2$ [−]	$\bar{t}$ [s]	σ [s]	$\bar{\sigma}^2$ [−]
Impulse 15 g	222	60	0.07	218*	23*	0.01*	214	55	0.07
Impulse 30 g	221	55	0.06	225	51	0.05	220	58	0.07
Impulse 60 g	223	62	0.08	232	64	0.08	219	58	0.07
Step-up 15 g/min	232	93	0.16	240	82	0.12	256	94	0.13
Step-up 30 g/min	221	50	0.05	241	69	0.08	222	65	0.08
Step-up 60 g/min	–	–	–	–	–	–	–	–	–
Step-down 15 g/min	219	80	0.13	234	78	0.11	222	72	0.11
Step-down 30 g/min	218	62	0.08	230	71	0.10	220	70	0.10
Step-down 60 g/min	214	68	0.10	222	69	0.10	215	67	0.10

*A stable plateau was not reached

For the impulse, step-up and step-down inputs, the mean residence times range from 214 to 232, 221 to 256, and 223 to 238 s, respectively. The standard deviations range from 51 to 64, 50 to 94 and 62 to 80 s, respectively. The mean residence time is similar for the impulse and step-down inputs, while the standard deviation is slightly different between the two inputs. The properties obtained from the step-up inputs differ significantly between the two tracer quantities and the impulse and step-down results.

The percentiles can be read directly from the cumulative residence time and wash-out function. For the RTD, the percentiles can be calculated as the percentage of the area under the curve. On average, the 1st percentile is 150 s, the 5th percentile 159 s, the 50th percentile (the median) 207 s, the 95th percentile 339 s, and the 99th percentile 410 s.

The presented DIP technique showed good repeatability when impulse and step-down inputs were applied, as shown by the relatively low variation in mean and standard deviations between experiments. Furthermore, the results are similar for most tracer concentrations, indicating that the amount of tracer material does not significantly influence the RTD of this specific combination of mortar and system. However, a significant difference exists for step inputs with high tracer concentrations. Here, there is an overshoot in the response, most likely due to the by-passing of the tracer material through the system. A possible explanation is that for impulse and step-up inputs with higher tracer concentrations, the added low-viscosity tracer is improperly mixed with the present high-viscosity mortar. Therefore, the tracer passed down through the gaps left by the mixer quicker than the mortar. Over time, the two fluids do mix, and the concentration stabilizes. This effect was not observed for the impulse inputs since the used concentrations were significantly lower. This effect cannot occur for step-down responses since there is no significant difference between viscosities in the mixing chamber.

Even though the amount of tracer material does not influence the RTD for most inputs, the original process was changed since the pumping pressure drops when the tracer concentration is above 0.4%, as shown in Fig. 13. This might be different for other combinations of materials and systems. Therefore, a minimum amount of tracer material should be applied, and monitoring at least one process value related to the material properties is recommended to measure a possible change. The amount of tracer material can still be reduced for the presented method, even though the original process was not changed for tracer contractions up to 0.4%, indicated by no significant change in pumping pressure for this concentration. For the lowest applied impulse of 15 g, the maximum estimated tracer concentration is 0.3%, corresponding to an SNR of roughly 70. Usually, an SNR of three is recommended [31] to detect a difference. However, the intermediate levels must also be detected sufficiently to obtain an RTD accurately. Therefore, an SNR in the order of thirty is expected to be required, corresponding to ten confidently detected differences. For the presented case, the impulse size can be reduced to 10 or 5 g, resulting in an SNR of ~ 50 and ~ 40, respectively, and a maximum water-to-solids percentages of 15.2% and 15.1% by weight.

These impulse sizes only contain 150 and 75 mg RhB powder.

The mean residence time $\bar{t}$ is around 220 s and the average mortar mass flow rate is 6 kg/min. From this, the volume can be estimated since $\bar{t} = V/Q$. The total mass in the system is around 22 kg; assuming the material's density is 2.1 kg/dm^3, the total volume V is around 10 L and the volumetric flow rate Q is around 2.9 l/min. The 130–140 s of dead time corresponds to a system volume of around 6 L. This volume roughly matches the volume of the hose and the additional pipes—the remaining volume of around 4 L matches the volume of the second mixing chamber of the mixer pump. Combined with the exponential decay of the RTD after the peak at 130–140 s, it suggests that for the examined material, the mixing chamber behaves as and can be modeled as an ideal continuous stirred tank reactor and the remaining hose and piping system as a plug flow reactor.

The mean residence time can be estimated by knowing the volume and flow rate. However, this gives no information about the spread in the residence time and how long a typical particle stays inside a system. Therefore, the variance σ^2 is a parameter to mention and use for comparison. Besides that, the percentiles of the RTD should be reported. Material scientists and chemical engineers can directly use these values since they indicate the time a percentage of a particle stays inside a system. From a control engineering perspective, these values indicate the time material is completely changed when, for instance, the water dosing is altered in case the tracer is applied at the water inlet. For the tested combination, the material changed by 5% after 159 s, while it took 339 s to obtain a change of 95%. To consider a material that is completely changed, the threshold of 99% is a good indicator.

The wavy pattern at the plateaus occurred due to continuously dosing the tracer material while the mortar was dosed in batches with an interval of 15–20 s. This periodic dosing of batches results in volume fluctuations in the second mixing chamber, and therefore, a continuous flow of tracer material results in fluctuations in the tracer concentration. The results from the step inputs can be improved by simultaneously dosing the tracer material with the mortar. Even though the synced dosing of tracer material would remove the wavy pattern, plateaus would still occur at the same interval. These plateaus would occur since no new mortar and tracer material would have been added to the mixing chamber between batches, keeping the tracer concentration constant until a new batch would be added.

To compare the different input types, the calculated properties are listed in Table 1. This is the only method for comparison since residence time functions can only be converted to one another if the system is linear time-invariant. For the lower tracer contents, the obtained properties from the different input types only differ slightly, which indicates that any input type could be used to quantify the function properties for the examined material-system combination. The time variance combined with continuous dosing of tracer material might explain the slight differences between the calculated properties of the various input types. These differences might not be significant since the interval between batches is 15–20 s while the median residence time is hundreds of seconds. For a linear time-invariant system, the residence time functions *can* be converted to one another, which makes the used input type even less relevant since any property and function can be obtained from any input type. However, Levenspiel [16] advises the impulse inputs since deviations in the RTD are less visible in the cumulative and wash-out function. Furthermore, for time-variant systems, we recommend selecting the input type that directly provides the most relevant information for the application. For example, impulse inputs can be used to obtain the RTD, which is relevant when studying the time-dependent material behavior in the system, and step inputs can be used when determining the response to a change in system settings.

5 Conclusion

This paper shows that a dye tracer experiment using a DIP technique is a cost-effective, practical and accurate method to measure the residence time functions in continuous concrete processing. Only an industrial camera, a lens, a polarization filter and a polarized light source are needed to detect the tracer dye. Furthermore, the experiment is performed in-line, which allows for the integration of the experiment into automated workflows for quality and process control. The color dye was detected with a high sample rate, allowing for a high-resolution measurement

of the tracer concentration. A high SNR was obtained by considering the chroma color plane distance in the CIELAB color space. A calibration curve was used to estimate the tracer concentration from the chroma color place distance. Validation of the experiment on a 3D concrete printing system in combination with a printable mortar shows that, for low tracer quantities, no significant influence of the tracer on the original process was observed. At high tracer quantities, an impact was observed for the step-up inputs. The tracer quantity can be significantly reduced since the lowest quantities provided an SNR of around 70, while an SNR of around 30 is expected to be sufficiently accurate.

Even though it has been shown that the experiment is easy to implement, some improvements can be made and need to be investigated. First, since the tracer material used dissolves in water, it only traces the water phase. Therefore, the RTD does not represent the RTD of the complete composition if segregation occurs. Such segregation, for example, could be induced by flow-induced migration of large particles to the core of the hose, leading to the formation of a lubrication layer with relatively higher water and fine particle content compared to the core of the hose [32]. Flow-induced migration increases for lower viscosity and lower yield stress materials pumped at a higher flow rate through a hose with a smaller diameter [33]. In such a case, the bulk of the material could have a more narrow RTD than indicated by the tracer measurement of the water phase. If the RTD of the water phase is close to a plug flow, one can conclude that migration effects are minimal. Otherwise, a complete look into the flow behavior of the material in the system could be obtained by tracing all the time-dependent material components, such as cement and additives. By comparing the results to the currently presented method, segregation could be identified for different flow typologies, and the effect of a mismatch between the material component's RTDs could be studied. Tracing the cement particles could, for example, be done with a pigment that binds to or behaves as the cement particles. Tracing based on DIP would become more difficult for larger particles since the cement paste covers them, obstructing detection. However, these are of lesser interest in most cases since they do not show time-dependent behavior. Second, the tracer concentration was estimated based on the surface color. Therefore, the mortar must be homogenized just before detection to ensure that the surface color represents the intensity of the entire filament cross-section. The mortar was homogenized in this study by placing helical static mixing elements before the nozzle with the detection device. However, this might not be possible for materials with high viscosity or yield stress. Third, the dye tracer experiment might be less effective on materials that have a dark appearance. Dark colors are more challenging to stain with a dye or pigment. Higher tracer concentrations are likely needed to measure a significant color difference for these materials, which can influence the process and thus affect the RTD.

6 Outlook

The authors encourage the application of the presented dye tracer experiment on various materials and systems, as well as the development of alternative tracer experiments, to detect any possible bias.

First, to compare various combinations of materials and systems, we propose to present the RTD curve and the RTD properties in combination with the mortar flow rate. We consider the mean, variance, dimensionless variance, and the 5th, 50th and 95th percentiles as suitable candidates. The 1st and 99th percentile can also be considered depending on the application. Even though it is not always possible to obtain the RTD curve due to the selection of input type, the properties can always be calculated with the theory summarized in this paper.

Second, we propose reporting the sample rate, SNR, and tracer concentrations to compare alternative tracer experiments or variants using the presented method. The SNR for specific tracer concentrations is especially important since the detection device, tracer material, and bulk material influence this. Additionally, we recommend checking if adding tracer material does not influence the original process by monitoring at least one process value related to the material properties, such as the pumping pressure, required mixing power or viscosity.

Acknowledgements This publication is part of the project "*Additive manufacturing of functional construction materials on-demand*" (with project number 17895) of the research program "*Materialen NL: Challenges 2018*" which is financed by the Dutch Research Council (NWO). Furthermore, this publication is part of the project "*Parametric mortar design and*

control of system parameters" funded by Saint-Gobain Weber Beamix. We thank m-tec mathis technik gmbh for supplying the mixer pump and Siemens Digital Industries for technical support. The authors thank the personnel from the Structures Laboratory at Eindhoven University of Technology, particularly Eric Wijnen, for the support during the development of the experiment.

Declarations

Conflict of interest The authors declare that they have no competing interests.

References

1. Fritschi L (2016) Smart dynamic casting-a digital fabrication method for non-standard concrete structures. doi: https://doi.org/10.3929/ETHZ-A-010800371
2. Khoshnevis B, Hwang D, Yao KT, Yeh Z (2006) Mega-scale fabrication by contour crafting. Int J Ind Syst Eng 1(3):301–320. https://doi.org/10.1504/IJISE.2006.009791
3. Neudecker S, Bruns C, Gerbers R, Heyn J, Dietrich F, Dröder K, Raatz A, Kloft H (2016) A new robotic spray technology for generative manufacturing of complex concrete structures without formwork. Procedia CIRP 43:333–338. https://doi.org/10.1016/J.PROCIR.2016.02.107
4. Suiker ASJ (2018) Mechanical performance of wall structures in 3D printing processes: theory, design tools and experiments. Int J Mech Sci 137:145–170. https://doi.org/10.1016/j.ijmecsci.2018.01.010
5. Wolfs RJM, Suiker ASJ (2019) Structural failure during extrusion-based 3D printing processes. Int J Adv Manuf Technol 104(1–4):565–584. https://doi.org/10.1007/s00170-019-03844-6
6. Suiker ASJ, Wolfs RJM, Lucas SM, Salet TAM (2020) Elastic buckling and plastic collapse during 3D concrete printing. Cem Concr Res 135:106016. https://doi.org/10.1016/j.cemconres.2020.106016
7. Palacios M, Flatt RJ (2016) Working mechanism of viscosity-modifying admixtures. Science and technology of concrete admixtures. Elsevier, Amsterdam, pp 415–432
8. Aïtcin P-C (2016) "Accelerators", in science and technology of concrete admixtures. Elsevier, Amsterdam, pp 405–413
9. Tao Y, Rahul AV, Lesage K, Yuan Y, Van Tittelboom K, De Schutter G (2021) Stiffening control of cement-based materials using accelerators in inline mixing processes: Possibilities and challenges. Cem Concr Compos 119:103972. https://doi.org/10.1016/J.CEMCONCOMP.2021.103972
10. Wangler T, Pileggi R, Gürel S, Flatt RJ (2022) A chemical process engineering look at digital concrete processes: critical step design, inline mixing, and scaleup. Cem Concr Res 155:106782. https://doi.org/10.1016/J.CEMCONRES.2022.106782
11. Roussel N (2018) Rheological requirements for printable concretes. Cem Concr Res 112:76–85. https://doi.org/10.1016/j.cemconres.2018.04.005
12. Perrot A, Pierre A, Nerella VN, Wolfs RJM, Keita E, Nair SAO, Neithalath N, Roussel N, Mechtcherine V (2021) From analytical methods to numerical simulations: A process engineering toolbox for 3D concrete printing. Cem Concr Compos 122:104164. https://doi.org/10.1016/J.CEMCONCOMP.2021.104164
13. Mechtcherine V, Fataei FP, Bos F, Buswell R, Leal da Silva WR, Keita E, Krauss HW, Lowke D, Perrot A, Nerella VN, Roussel N, Sonebi M, Wangler T, Weger D, Wolfs R (2022) Digital fabrication with cement-based materials: underlying physics. In: Roussel N, Lowke D (eds) Digital fabrication with cement-based materials: state-of-the-art report of the RILEM TC 276-DFC. Springer International Publishing, Cham, pp 49–98. https://doi.org/10.1007/978-3-030-90535-4_3
14. Wangler T, Scotto F, Lloret-Fritschi E, Flatt RJ (2019) Residence time distributions in continuous processing of concrete. RILEM Bookseries. Springer, Cham, pp 448–456
15. Levenspiel O (1999) Chemical reaction engineering. Wiley & Sons
16. Levenspiel O (2012) Tracer technology: modeling the flow of fluids. Springer New York
17. Heller W (1990) Prozessanalyse von Mischsystemen der betonherstellung mit hilfe der radionuklid-tracertechnik
18. Bos D, Wolfs R (2023) A quality control framework for digital fabrication with concrete. RILEM Techn Lett 8:106–112. https://doi.org/10.21809/rilemtechlett.2023.181
19. Danckwerts PV (1953) Continuous flow systems. Chem Eng Sci 2(1):1–13. https://doi.org/10.1016/0009-2509(53)80001-1
20. Nauman EB (2008) Residence time theory. Ind Eng Chem Res 47(10):3752–3766. https://doi.org/10.1021/ie071635a
21. Ruot B, Plassais A, Olive F, Guillot L, Bonafous L (2009) TiO_2-containing cement pastes and mortars: measurements of the photocatalytic efficiency using a rhodamine B-based colourimetric test. Sol Energy 83(10):1794–1801. https://doi.org/10.1016/J.SOLENER.2009.05.017
22. Aigner M, Lepschi A, Aigner J, Garmendia I, Miethlinger J (2015) Experimental study and verification of the residence time distribution using fluorescence spectroscopy and color measurement. AIP Conf Proc 1664(1):100005. https://doi.org/10.1063/1.4918472

23. Wesholowski J, Berghaus A, Thommes M (2018) Inline determination of residence time distribution in hot-melt-extrusion. Pharmaceutics 10(2):49. https://doi.org/10.3390/PHARMACEUTICS10020049
24. Kumar A, Ganjyal GM, Jones DD, Hanna MA (2006) Digital image processing for measurement of residence time distribution in a laboratory extruder. J Food Eng 75(2):237–244. https://doi.org/10.1016/J.JFOODENG.2005.04.025
25. Bi C, Jiang B, Li A (2007) Digital image processing method for measuring the residence time distribution in a plasticating extruder. Polym Eng Sci 47(7):1108–1113. https://doi.org/10.1002/pen.20793
26. Wahl PR, Hörl G, Kaiser D, Sacher S, Rupp C, Shlieout G, Breitenbach J, Koscher G, Khinast JG (2018) In-line measurement of residence time distribution in melt extrusion via video analysis. Polym Eng Sci 58(2):170–179. https://doi.org/10.1002/PEN.24544
27. Choi M, Roussel N, Kim Y, Kim J (2013) Lubrication layer properties during concrete pumping. Cem Concr Res 45(1):69–78. https://doi.org/10.1016/J.CEMCONRES.2012.11.001
28. Fataei S, Secrieru E, Mechtcherine V (2020) Experimental insights into concrete flow-regimes subject to shear-induced particle migration (SIPM) during pumping. Materials 13(5):1233. https://doi.org/10.3390/MA13051233
29. Thermo Fisher Scientific, "A13572 Rhodamine B product specification." Accessed: Apr. 11, 2022. [Online]. Available: https://alfaaesar.com/en/prodspec/A13572
30. Prenting MM, Bin Dzulfida MI, Dreier T, Schulz C (2020) Characterization of tracers for two-color laser-induced fluorescence liquid-phase temperature imaging in sprays. Exp Fluids 61(3):1–15. https://doi.org/10.1007/S00348-020-2909-9/FIGURES/10
31. Skoog DA, Holler FJ, Crouch SR (2018) *Principles of instrumental analysis seventh edition*. Cengage learning
32. Spangenberg J, Roussel N, Hattel JH, Stang H, Skocek J, Geiker MR (2012) Flow induced particle migration in fresh concrete: theoretical frame, numerical simulations and experimental results on model fluids. Cem Concr Res 42(4):633–641. https://doi.org/10.1016/j.cemconres.2012.01.007
33. Cox RG, Hsu SK (1977) The lateral migration of solid particles in a laminar flow near a plane. Int J Multiph Flow 3(3):201–222. https://doi.org/10.1016/0301-9322(77)90001-5